HEPATOLOGY

HEPATOLOGY, VOL. 71, NO. 4, 2020

A Bile Duct-on-a-Chip With Organ-Level Functions

Yu Du,[1,8] Gauri Khandekar,[1,8] Jessica Llewellyn ,[1,8] William Polacheck,[2-4] Christopher S. Chen,[3,5,8] and Rebecca G. Wells[1,6-8]

BACKGROUND AND AIMS: Chronic cholestatic liver diseases, such as primary biliary cholangitis (PBC) and primary sclerosing cholangitis (PSC), are frequently associated with damage to the barrier function of the biliary epithelium. Here, we report on a bile duct-on-a-chip that phenocopies not only the tubular architecture of the bile duct in three dimensions, but also its barrier functions.

APPROACH AND RESULTS: We showed that mouse cholangiocytes in the channel of the device became polarized and formed mature tight junctions, that the permeability of the cholangiocyte monolayer was comparable to *ex vivo* measurements, and that cholangiocytes in the device were mechanosensitive (as demonstrated by changes in calcium flux under applied luminal flow). Permeability decreased significantly when cells formed a compact monolayer with cell densities comparable to those observed *in vivo*. This device enabled independent access to the apical and basolateral surfaces of the cholangiocyte channel, allowing proof-of-concept toxicity studies with the biliary toxin, biliatresone, and the bile acid, glycochenodeoxycholic acid. The cholangiocyte basolateral side was more vulnerable than the apical side to treatment with either agent, suggesting a protective adaptation of the apical surface that is normally exposed to bile. Further studies revealed a protective role of the cholangiocyte apical glycocalyx, wherein disruption of the glycocalyx with neuraminidase increased the permeability of the cholangiocyte monolayer after treatment with glycochenodeoxycholic acid.

CONCLUSIONS: This bile duct-on-a-chip captured essential features of a simplified bile duct in structure and organ-level functions and represents an *in vitro* platform to study the pathophysiology of the bile duct using cholangiocytes from a variety of sources. (Hepatology 2020;71:1350-1363).

Chronic cholestatic liver diseases, such as primary biliary cholangitis (PBC) and primary sclerosing cholangitis (PSC), are often associated with alterations in the tight junctions of bile duct epithelial cells (cholangiocytes). Data from mouse models similarly suggest that impaired tight junction integrity plays an important role in the pathogenesis of cholangiopathies.[1-6] Most *in vitro* research on biliary physiology and pathology, however, uses cells either cultured in two-dimensional (2D) monolayers or as organoids in three-dimensional (3D) extracellular matrix (ECM).[7-11] These conventional methods fail to replicate many key aspects of bile duct structural organization or to recapitulate important tissue-level integrated physiological functions, such as forming a protective barrier and compartmentalizing bile.

Microfluidic organs-on-chips can overcome some of these limitations.[12] Soft lithography, which is used

Abbreviations: 2D, two-dimensional; 3D, three-dimensional; ASBT, apical sodium-dependent bile salt transporter; BSA, bovine serum albumin; Cy, cyanine; DAPI, 4′,6-diamidino-2-phenylindole; DMEM, Dulbecco's modified Eagle's medium; ECM, extracellular matrix; EHBD, extrahepatic bile duct; FITC, fluorescein isothiocyanate; GCDC, glycochenodeoxycholic acid; K19, keratin 19; PBC, primary biliary cholangitis; PBS, phosphate-buffered saline; PDMS, polydimethylsiloxane; PFA, paraformaldehyde; PSC, primary sclerosing cholangitis; RT, room temperature; SBA, soybean agglutinin; SNA, Sambucus nigra lectin; ZO-1, zona occludens 1.

Received March 25, 2019; accepted August 22, 2019.

Additional Supporting Information may be found at onlinelibrary.wiley.com/doi/10.1002/hep.30918/suppinfo.

Supported by grant R56 DK119290 from the National Institutes of Diabetes and Digestive and Kidney Diseases (to R.G.W.), R01 EB08396 from the National Institute of Biomedical Imaging and Bioengineering, the Fred and Suzanne Biesecker Foundation for Pediatric Liver Diseases at the Children's Hospital of Philadelphia, and the Center for Engineering MechanoBiology (CEMB), an NSF Science and Technology Center, under grant agreement CMMI: 15-48571. W.J.P. acknowledges support from a Ruth L. Kirchstein National Research Service Award (F32 HL129733) and from the NIH through the Organ Design and Engineering Training program (T32 EB16652).

View this article online at wileyonlinelibrary.com.

DOI 10.1002/hep.30918

Potential conflict of interest: Nothing to report.

to design organs-on-chips, allows control of surface features over a range of physiologically relevant scales. Organs-on-chips can mimic aspects of the physiology of cell-cell and cell-ECM junctions in tissues, including the alveolar-capillary interface,[13] the blood–brain barrier,[14-16] and liver sinusoids,[17] in a controllable way, allowing both high-resolution imaging and biochemical and metabolic analyses in real time. The technology has great potential to advance the study of tissue development, physiology, and pathophysiology.

To capture the structure and environment of the bile ducts, we used organ-on-chip technology with a microengineered bile duct with controllable architecture and surrounding matrix. We demonstrate that a self-organized cholangiocyte-lined channel faithfully recapitulates key functions of the bile duct and enables us to study the barrier function of the cholangiocyte monolayer quantitatively and independently from either the apical or basolateral side. As a proof of concept, we use this model to show that the cholangiocyte apical glycocalyx plays a protective role and to demonstrate, through changes in cholangiocyte calcium flux in response to applied luminal flow, that cholangiocytes are mechanosensitive.

Materials and Methods

CELL ISOLATION AND CULTURE

The small cholangiocyte cell line was originally isolated from normal mice (BALB/c) and immortalized by transfection with the SV40 large-T antigen.[18] Primary cholangiocytes were isolated from extrahepatic bile ducts (EHBDs) of wild-type adult mice (BALB/c) as described.[19] Each batch of primary cholangiocytes consisted of pooled cells isolated from 3-5 mice. Cells were cultured in low-glucose Dulbecco's modified Eagle's medium (DMEM; Thermo Fisher Scientific, Waltham, MA), supplemented as reported.[18-20]

FABRICATION OF THE BILE DUCT-ON-A-CHIP

Microfluidic devices were fabricated using soft lithography as described[21,22] (Fig. 1A). Polydimethylsiloxane (PDMS; Sylgard 184; Dow-Corning, Midland, MI) devices were treated with 0.01% (v/v) poly-L-lysine for 1 hour and 0.5% (v/v) glutaraldehyde for 20 minutes to promote collagen adhesion. After the devices were washed overnight in water and for 30 minutes in 70% ethanol, steel acupuncture needles (160-μm diameter; Seirin, Kyoto, Japan) were inserted and the devices were then sterilized under UV for 20 minutes. A solution of 2.5 mg/mL of rat tail type 1 collagen (Thermo Fisher Scientific), 1× DMEM medium, 10 mM of HEPES, 0.1 M of NaOH, and $NaHCO_3$ (0.035% w/v) was infused by the side ports and allowed to polymerize for 20 minutes at 37°C. Needles were removed to form channels, which were then coated with 100 μg/mL of laminin (a major protein in the biliary basement membrane) overnight (by the large reservoir ports) at 37°C. A suspension of 0.5 million/mL of cholangiocytes was introduced into the reservoir ports. Cells were allowed to adhere

ARTICLE INFORMATION:

From the [1]Division of Gastroenterology, Department of Medicine, Perelman School of Medicine at the University of Pennsylvania, Philadelphia, PA; [2]The Wyss Institute for Biologically Inspired Engineering, Harvard University, Boston, MA; [3]The Biological Design Center and Department of Biomedical Engineering, Boston University, Boston, MA; [4]Joint Department of Biomedical Engineering, University of North Carolina at Chapel Hill and North Carolina State University, Chapel Hill, NC; [5]Tissue Microfabrication Laboratory, Department of Biomedical Engineering, Boston University, Boston, MA; [6]Department of Bioengineering, School of Engineering and Applied Sciences, The University of Pennsylvania, Philadelphia, PA; [7]Department of Pathology and Laboratory Medicine, Perelman School of Medicine at the University of Pennsylvania, Philadelphia, PA; [8]Center for Engineering MechanoBiology, The University of Pennsylvania, Philadelphia, PA.

ADDRESS CORRESPONDENCE AND REPRINT REQUESTS TO:

Rebecca G. Wells, M.D.
Department of Medicine (GI)
Perelman School of Medicine, University of Pennsylvania
905 BRB II/III
421 Curie Boulevard
Philadelphia, PA 19104-6140
E-mail: rgwells@pennmedicine.upenn.edu
Tel.: +1-215-573-1860

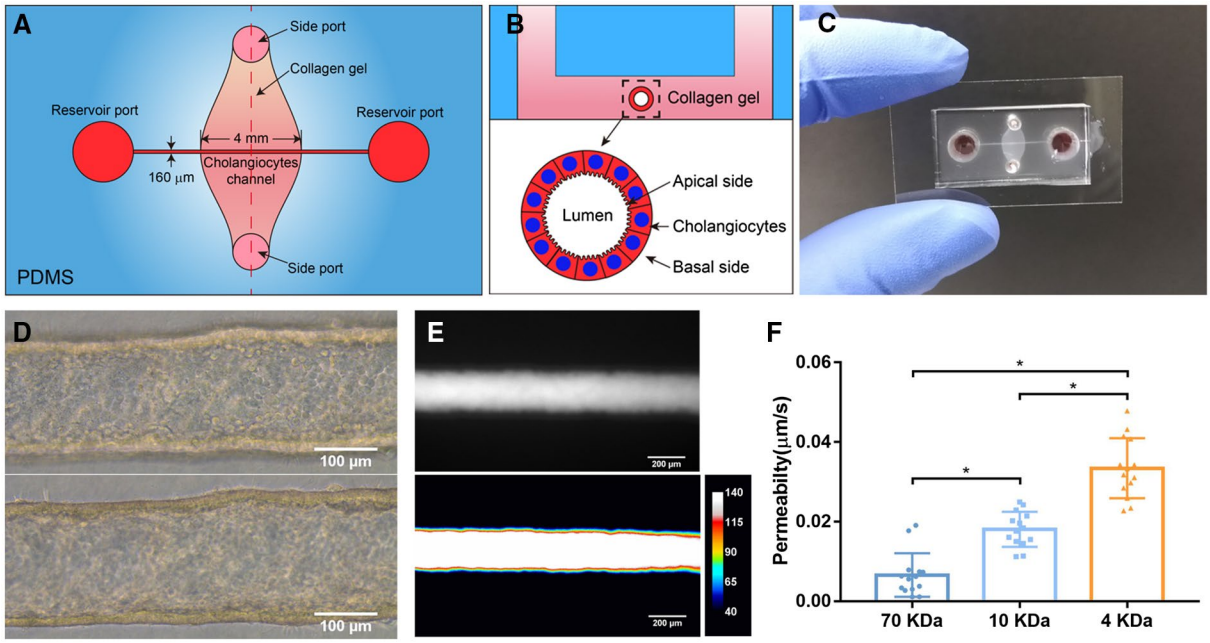

FIG. 1. Fabrication and characterization of a 3D biomimetic bile duct-on-a-chip. (A) Schematic of top view of the bile duct-on-a-chip. (B) Schematic of the device in cross-section. (C) Image of an actual bile duct-on-a-chip, top view. (D) Representative bright-field image of the channel (bottom [upper panel] and middle [lower panel]) lined by a layer of mouse cholangiocytes (cell line). Scale bar, 100 µm. (E) Representative image of FITC-dextran (70 kDa) in the channel, imaged after 10 minutes (upper panel), with pseudo color shown in lower panel. Scale bar, 200 µm. (F) Permeability of the cholangiocyte (cell line)-lined channel to FITC-dextran (70, 10, and 4 kDa), n = 14 devices, each device tested sequentially with FITC-dextran from 70 to 4 kDa. All data are presented as mean ± SD; **P* < 0.05.

to the top surface of the channel for 2 minutes; devices were then flipped to allow cells to adhere to the bottom surface of the channel for 5 minutes. (Times were determined empirically to yield an even cell coating of the channel and sufficient adhesion to permit rinsing the channel.) Nonadherent cells were removed by rinsing with cell-culture medium, and the devices were filled with fresh medium. Devices were maintained at 37°C (5% CO_2) for 7 days on a rocker at 5 rpm with daily medium changes until the development of compact monolayers.

PERMEABILITY MEASUREMENTS

To measure the permeability of the cholangiocyte monolayers in the device, fluorescent dextran (70, 10, and 4 kDa, labeled with fluorescein isothiocyanate [FITC]; Sigma-Aldrich, St. Louis, MO) in phosphate-buffered saline (PBS) was introduced into the devices at a concentration of 20 µg/mL. Diffusion of the dextran was imaged in real time with an EVOS FL Auto 2 Imaging System (Thermo Fisher Scientific) at 10× magnification. The diffusive permeability coefficient was calculated by measuring the flux of dextran into the collagen gel and fitting the resulting diffusion profiles to a dynamic mass conservation equation, as described.[21,23]

IMMUNOSTAINING AND LECTIN STAINING

Cholangiocyte monolayers in the device were fixed with 4% paraformaldehyde (PFA) at 37°C for 20 minutes with rocking. Cells were rinsed 3× with PBS and permeabilized with 0.1% Triton X-100 for 3 days, then blocked with 2% bovine serum albumin (BSA; Sigma-Aldrich) in PBS at 4°C overnight with rocking. Primary antibodies, together with 4′,6-diamidino-2-phenylindole (DAPI; Thermo Fisher Scientific) diluted in 2% BSA in PBS, were incubated overnight at 4°C and rinsed 3× with PBS for 5 minutes each with rocking, followed by an overnight rinse. Secondary antibodies were diluted in 2% BSA in PBS, incubated overnight at 4°C, and rinsed 3× with PBS for

5 minutes each on a rocker, followed by an overnight rinse. Primary antibodies and the concentrations used are listed in Supporting Table S1. Cyanine (Cy)3- and Cy5-conjugated secondary antibodies were used at 1:400 (Vector Laboratories, Burlingame, CA).

Extrahepatic bile ducts were frozen in O.C.T. (Tissue-Tek; VWR, Bridgeport, NJ). Sections (5 μm thick) were brought to room temperature and fixed in 10% neutral buffered formalin for 4 minutes. Tissue was blocked with StartingBlock T20/PBS Blocking Buffer (Thermo Fisher Scientific) before being incubated overnight with keratin 19 (K19) primary antibody (1:100; Troma III; DSHB, Iowa City, IA) in staining buffer (0.2% Triton X-100, 0.1% BSA, in PBS) at 4°C. Cy2 AffiniPure Donkey Anti-Rat IgG (H+L; 1:500; Jackson ImmunoResearch Lab, West Grove, PA) was then used as the secondary antibody and incubated for 1 hour at room temperature (RT).

For Sambucus nigra (SNA) and soybean agglutinin (SBA) lectin staining, cholangiocytes were fixed with 4% PFA at 37°C for 20 minutes with rocking. Cells were rinsed with PBS for 1 hour, then blocked with 1× Carbo-Free Blocking Solution (Vector Laboratories) for 1 hour at RT on a rocker. After 3× 15-minute PBS rinses, cells were incubated with SBA-FITC or SNA-Cy5 (Vector Laboratories) at 20 μg/mL for 1 hour at RT with rocking. Cells were rinsed with PBS for 1 hour, then the channel was filled with mounting medium containing DAPI (Vector Laboratories). Images were acquired using a SCTR Leica confocal microscope and Leica application suite (LAS X; Leica, Buffalo Grove, IL).

TERMINAL DEOXYNUCLEOTIDYL TRANSFERASE DUTP NICK END LABELING STAINING

Cholangiocyte monolayers in the device were fixed with 4% PFA at 37°C for 20 minutes with rocking. Cells were rinsed 3× with PBS and permeabilized with 0.1% Triton X-100 overnight, then were stained using the In Situ Cell Death Detection Kit (Roche, Basel, Switzerland).

PARTICLE IMAGING VELOCIMETRY

To measure flow velocities, 0.2 μm of carboxylate-modified microbeads (Thermo Scientific) labeled with red fluorescence (580/605) were diluted in PBS to a concentration of 4.55×10^8/mL, then continuously perfused into the device channel using a syringe pump (Braintree Scientific, Braintree, MA). The local velocity of the fluid flowing through the channel was calculated by tracking the movement of the fluorescent particles frame by frame as described.[17] The wall shear stress was determined based on the assumption that the fluid field in the channel can be approximated as a steady pipe flow (Eq. 1):

$$\tau = \frac{32\mu Q}{\pi D^3} \quad (1)$$

where τ is the wall shear stress, μ the viscosity, Q the flow rate, and D the channel diameter.

CALCIUM IMAGING

For calcium dye loading, cholangiocytes were incubated with 5 μM of Fluo4-AM solution (Thermo Fisher Scientific) and placed on a rocker for 2 hours at 37°C. Excess dye was washed away with Hanks' balanced salt solution (HBSS) before flow experiments. The bile duct-on-a-chip was connected to a syringe pump to apply shear flow with HBSS at 3.9 dyne/cm^2. Time-lapse images were acquired at 1-second intervals for 3 minutes using an Olympus IX81 spin disk confocal microscope (Olympus, Tokyo, Japan).

STATISTICAL ANALYSIS

Statistical significance was assessed using one-way analysis of variance. $P < 0.05$ was regarded as statistically significant and calculated with Prism software (version 7; GraphPad Software Inc., La Jolla, CA). All data are presented as mean ± SD. Sample size is indicated in the corresponding figure legends.

Results

FABRICATION OF THE BILE DUCT-ON-A-CHIP

In order to study the function of the apical and basal sides of cholangiocyte monolayers independently, we used a microfluidic device consisting of a PDMS support containing a cholangiocyte-lined channel

(4 mm in length, 160 μm in diameter) through a collagen plug; the apical and basal sides of the channel are accessible through separate ports (Fig. 1A-C). The device was designed as per previously described models of endothelium-lined, vascular-mimetic channels.[21,22] To maximize cholangiocyte adhesion, the lumen was coated with laminin (100 μg/mL) for 4 hours. The channels described here were seeded with a line of mouse cholangiocytes. Cholangiocytes in the channel formed a confluent and then compact epithelial monolayer after 7 days (Figs. 1D and Supporting Fig. S1).

To determine whether the bile duct-on-a-chip recapitulated the barrier function of the bile duct, we perfused the lumen with FITC-dextran ranging in size from 4 to 70 kDa (Supporting Fig. S2). There was no obvious leakage of fluorescent dextran into the collagen matrix even after 10 minutes (Fig. 1E). Quantification of permeability showed an increase as the molecular weight of the dextran decreased (Fig. 1F). The measured permeability of channels lined with a mouse small cholangiocyte cell line[18] fell within the range of that measured in *ex vivo* systems using insulin (5.8 kDa; 0.45 μm/s in rat and 0.012 μm/s in guinea pig).[24,25] This model of the bile duct thus mimics the barrier function of ducts *in vivo*.

CHARACTERIZATION OF THE BILE DUCT-ON-A-CHIP

We used immunofluorescence staining to characterize the cholangiocytes in the channel. F-actin staining showed that cholangiocytes grew into a compact monolayer, forming a cylindrical tube with two open ends connected to the large reservoirs (Fig. 2A,C). Cells maintained expression of the cholangiocyte marker, K19 (Fig. 2B) and demonstrated staining for zona occludens 1 (ZO-1; tight junction protein 1) and E-cadherin 1 (also known as cadherin 1) at cell-cell junctions (Fig. 2D,E), confirming the formation of tight junctions. Staining for the apical sodium-dependent bile acid transporter (ASBT) confirmed that cells in the bile duct-on-a-chip were polarized (Fig. 2F).

A SUPERCONFLUENT MONOLAYER IS REQUIRED FOR OPTIMAL BARRIER FUNCTION

Full barrier function required that cholangiocytes were not just confluent, but "superconfluent" and compact (Fig. 3A); as the cholangiocyte monolayer grew more dense, permeability decreased significantly (Fig. 3A,B). By F-actin staining, we confirmed that the permeability difference between what we term a confluent versus a compact monolayer was not the result of gaps in the monolayer (Fig. 3C). Cell height and height-to-width ratio were increased more than 2-fold in the compact compared to the confluent monolayer (Fig. 3D,F). To determine the cell density of cholangiocyte monolayers *in vivo*, we counted cell number as a function of monolayer length in normal adult mouse EHBD (Fig. 3E) and in confluent and compact devices. We found that compact monolayers were more dense than confluent ones, and that mice EHBD (Fig. 3E,F) had an even higher cell density. These results suggested that the biliary epithelium forms a dense, compact monolayer—beyond confluence—in order to form a mature barrier.

THE APICAL AND BASAL SURFACES OF THE MONOLAYER CAN BE ACCESSED INDEPENDENTLY

In order to determine whether the apical and basal surfaces of cholangiocytes in the device could be accessed independently, we applied FITC-dextran through either the large reservoir ports, which are directly connected to the lumen, or the small side ports, which connect to the basal surface of the monolayer through the collagen bulk. We found that FITC-dextran added through the reservoir ports remained within the lumen (Fig. 4A,B), making contact only with the apical side of the cholangiocytes in the device and unable to penetrate through the monolayer. Dextran applied by the side ports remained within the collagen plug, in contact with only the basal side of the monolayer (Fig. 4C,D).

Biliatresone is a plant isoflavonoid that is toxic to cholangiocytes and causes a syndrome mimicking the pediatric disease biliary atresia in neonatal livestock and larval zebrafish.[26] We previously demonstrated that biliatresone applied to the basal surface of a cholangiocyte spheroid causes mislocalization of the apical markers ZO-1 and E-cadherin and increases cholangiocyte monolayer permeability.[20] A limitation of these spheroid studies was that biliatresone could only be added to the basal surface. As a demonstration of

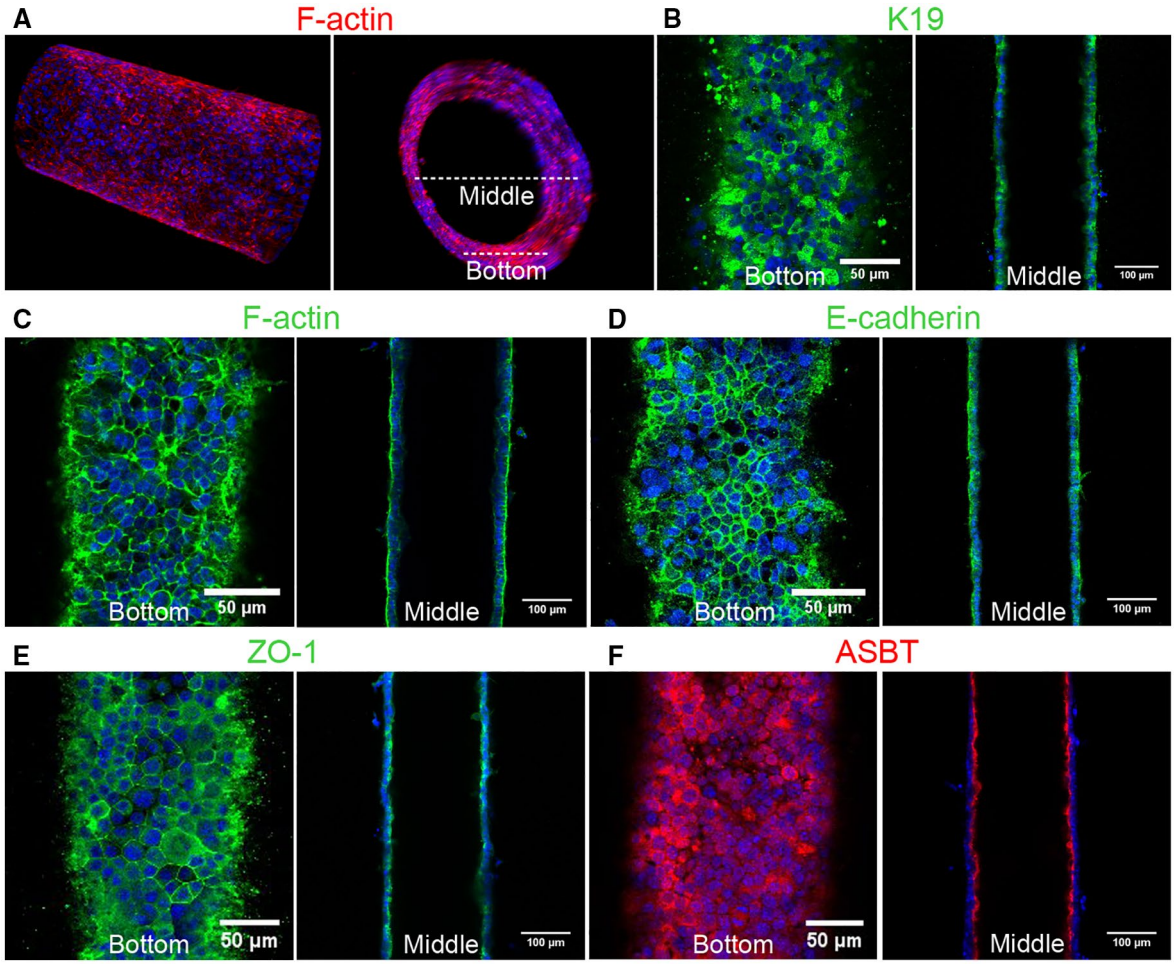

FIG. 2. Characterization of a channel lined with mouse cholangiocytes (cell line). (A) Representative confocal images of cholangiocytes in the bile duct-on-a-chip forming a monolayer within the cylindrical channel, stained for F-actin (red) and nuclei (DAPI; blue). Longitudinal (left panel) and cross-sectional (right panel) views. White dashed lines indicate the bottom surface and cross-section through the center shown in the remaining panels. (B-F) Immunofluorescent images across the bottom (left panels in B-F) and middle (right panels in B-F) of the channel stained with antibodies against (B) K19, (C) F-actin, (D) E-cadherin, (E) ZO-1, and (F) the ASBT. Nuclei shown by DAPI staining (blue). Images are representative of at least three independently constructed devices for each condition. Scale bars: 50 μm, left panels; 100 μm, right panels.

the potential use of the bile duct-on-a-chip device, we showed that biliatresone treatment caused cholangiocyte damage, as evidenced by increased permeability of monolayers in the device, and that this damage was worse with basal as opposed to apical administration (Fig. 4E).

Cholangiocytes are adapted to tolerate exposure to toxic bile at their apical surfaces, though it has been difficult to study in cell culture.[27] Impaired duct barrier function may lead to bile leakage through the monolayer and cause damage from the basolateral side, which is less tolerant of bile.[28-30] As a second illustration of the potential use of the bile duct-on-a-chip device, we exposed cholangiocytes to 1 mM of the bile acid glycochenodeoxycholic acid (GCDC) from either the apical or basal side. GCDC treatment caused significantly more damage, as defined by increased permeability without significant apoptosis (Supporting Fig. S3), when applied to the basal side rather than the apical side (Fig. 4F), suggesting that once bile leaks through the epithelial monolayer, it can cause additional damage through the basolateral side of the barrier, leading to a feedback loop of further damage and increased leakage.

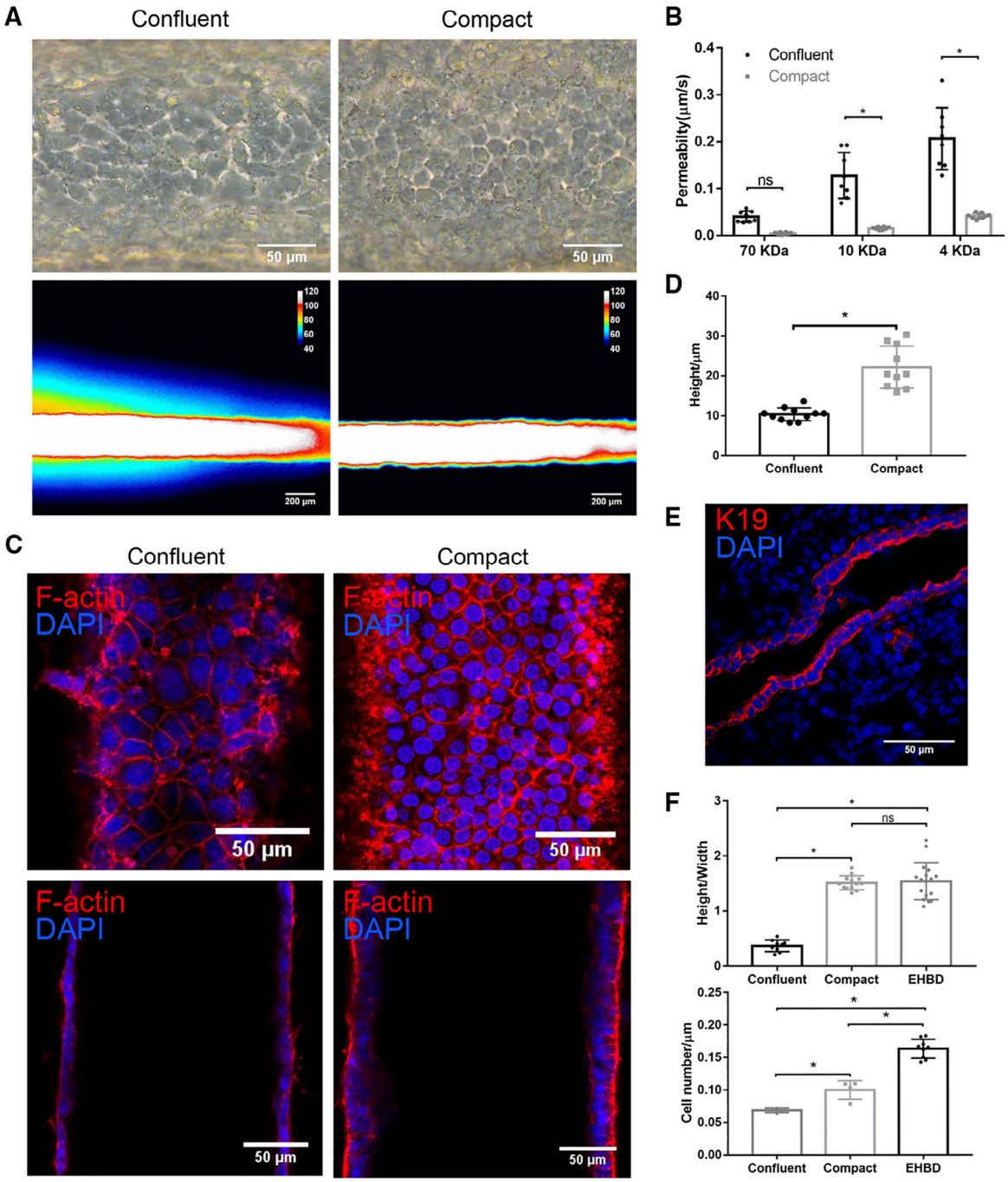

FIG. 3. Cholangiocyte monolayers require high confluency for mature barrier function. (A) Representative bright-field images (upper panels) and pseudo color images after FITC-dextran (4 kDa) perfusion for 2 minutes (lower panels) of confluent and compact cholangiocyte channels. Scale bar: 100 μm (upper panels), 200 μm (lower panels). (B) Permeability of confluent and compact cholangiocyte channel to FITC-dextran (70, 10, and 4 kDa), n = 8 devices. (C) Bottom (upper panels) and middle (lower panels) views of confluent and compact cholangiocyte monolayers in the devices, stained for F-actin (red) and nuclei (DAPI; blue). Scale bars, 50 μm. (D) Cell height of confluent and compact cholangiocyte monolayers in the devices, n ≥ 10. (E) Adult mouse extrahepatic bile duct, stained for K19 (red) and nuclei (DAPI; blue), representative images from n = 9. Scale bar, 50 μm. (F) Cell height/width ratio (upper panel) and cell density (lower panel) in confluent and compact cholangiocyte channels and mice EHBD, n = 4-9. Images are representative of at least three independent experiments. All data are presented as mean ± SD; $^*P < 0.05$.

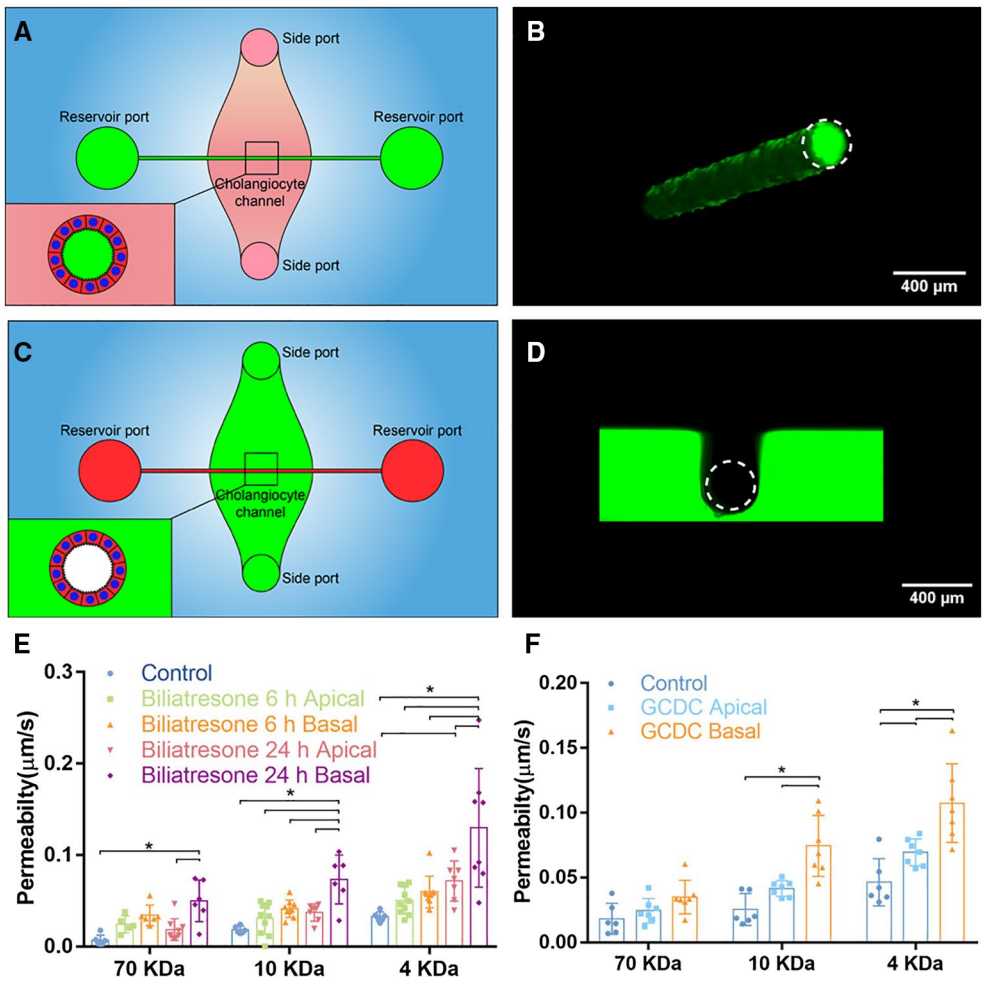

FIG. 4. The apical and basal surfaces of cholangiocytes can be treated independently. (A) Schematic showing access to the apical side of cholangiocytes through the reservoir ports. (B) Confocal image of FITC-dextran solution (green) in the lumen after administration through the reservoir ports. Scale bar, 400 μm. (C) Schematic showing access to the basal side of cholangiocytes through the side ports. (D) Confocal image of FITC-dextran solution (green) in the collagen bulk and surrounding, but not within, the lumen after administration through the side ports. Scale bar, 400 μm. (E) Diffusive permeability across monolayers treated with biliatresone by apical or basal surfaces for 6 or 24 hours, as measured using FITC-dextran (70, 10, and 4 kDa) in the lumen, n ≥ 6 devices for each condition. (F) Diffusive permeability across monolayers treated with 1 mM of GCDC by apical or basal surfaces for 1 hour, as measured using FITC-dextran (70, 10, and 4 kDa) in the lumen, n ≥ 6 devices for each condition. All data are presented as a mean ± SD; $^*P < 0.05$.

THE GLYCOCALYX PROTECTS CHOLANGIOCYTES FROM BILE-ACID–INDUCED DAMAGE

Cholangiocytes have an apical glycocalyx that protects them from bile acid toxicity.[31,32] We stained the apical surfaces of the cholangiocyte monolayer in the bile duct-on-a-chip using the lectin, SNA, which binds to $\alpha_{2\text{-}6}$-bound (terminal) sialic acid residues, and demonstrated that the sialic-acid–enriched glycocalyx was maintained in cholangiocytes in the device and was appropriately localized to the apical surface (Fig. 5A). We also stained cells in the channel with the lectin, SBA, which only detects carbohydrates *lacking* terminal sialic acid residues (Fig. 5E), confirming a lack of cholangiocyte staining at baseline (Fig. 5B). We then treated cells with neuraminidase, applied apically, to remove the terminal sialic acid. Posttreatment staining with SNA was minimal, while there was new staining with SBA, confirming the presence of apical sialic acid residues in untreated cells and the efficacy of neuraminidase in this system (Fig. 5C,D). To test the role

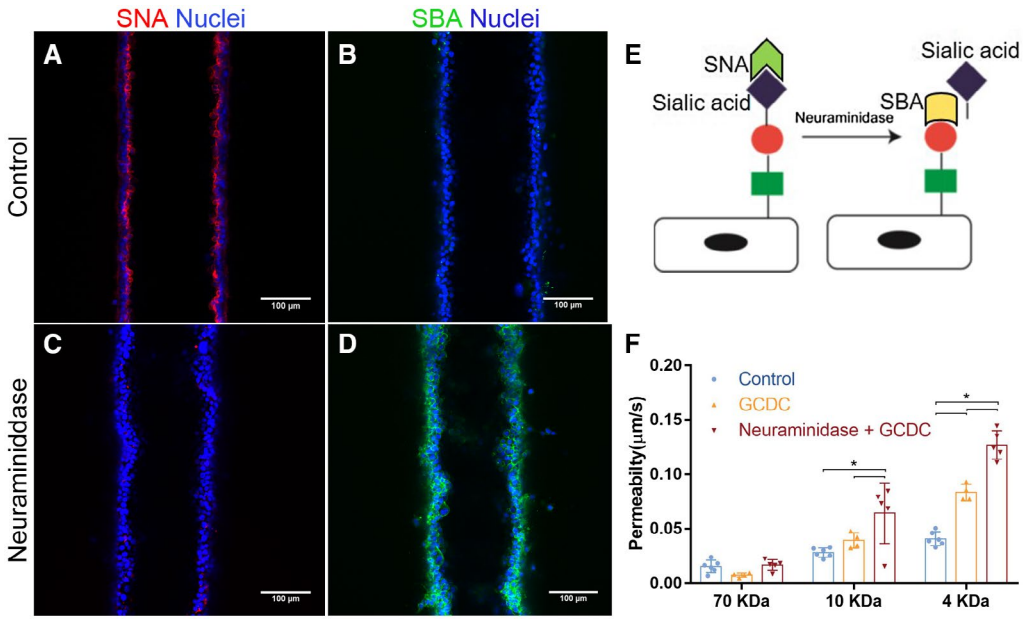

FIG. 5. An intact glycocalyx protects cholangiocytes from bile acids. (A-D) Staining using the lectins, SNA and SBA, in the bile duct-on-a-chip (A,B) before and (C,D) after neuraminidase treatment. Scale bars, 100 μm. (E) Schematic showing that SNA recognizes sialyated carbohydrates, and that removal of sialic acid is required for recognition by SBA. (F) Diffusive permeability of devices treated with the bile acid, GCDC, with or without previous desialyation with neuraminidase, n = 4-6 devices for each condition. All data are presented as mean ± SD; $^*P < 0.05$.

of the glycocalyx in protecting cholangiocytes from bile acids, we perfused the device lumen with GCDC (1 mM) before or after treatment with neuraminidase, and then measured monolayer permeability. We found no effect of GCDC, with or without neuraminidase treatment, on permeability to 70-kDa FITC-dextran; however, GCDC alone increased the permeability to 4-kDa FITC-dextran, and GCDC exposure of neuraminidase-treated cholangiocytes increased permeability to both 4- and 10-kDa FITC-dextran (Fig. 5F). Taken together, these findings demonstrate that the cholangiocyte-lined channel is resistant to bile acid toxicity and that the glycocalyx plays a protective role.

CONSTRUCTION OF A BILE DUCT-ON-A-CHIP WITH PRIMARY MURINE EXTRAHEPATIC CHOLANGIOCYTES

To demonstrate that the bile duct-on-a-chip can be used with cells from various sources, we also used primary murine extrahepatic cholangiocytes. Primary cholangiocytes, like the cell line, formed a compact tubular monolayer (Supporting Fig. S4). Cells maintained stable expression of the cholangiocyte markers, K19 and epithelial cell adhesion molecule (Fig. 6A and Supporting Fig. S5D-F), and demonstrated staining for E-cadherin and ZO-1 at cell-cell junctions (Fig. 6C,D), confirming the formation of tight junctions. Staining for ASBT (Fig. 6B and Supporting Fig. S5A-C) and acetylated α-tubulin (Fig. 6E,F) confirmed that primary cholangiocytes in the bile duct-on-a-chip were ciliated and polarized over time.

FUNCTIONAL ANALYSIS OF THE PRIMARY BILE DUCT-ON-A-CHIP

In permeability assays, there was no visible leakage of 4-kDa FITC-dextran from the lumen even after 10 minutes (Fig. 7A; Supporting Movie S1). Permeability to 4-kDa FITC-dextran of primary cholangiocytes was around only 16% of that for the cholangiocyte cell line (Fig. 7B). Thus, the primary cell-lined device demonstrated even better barrier function than the device lined with the cholangiocyte cell line.

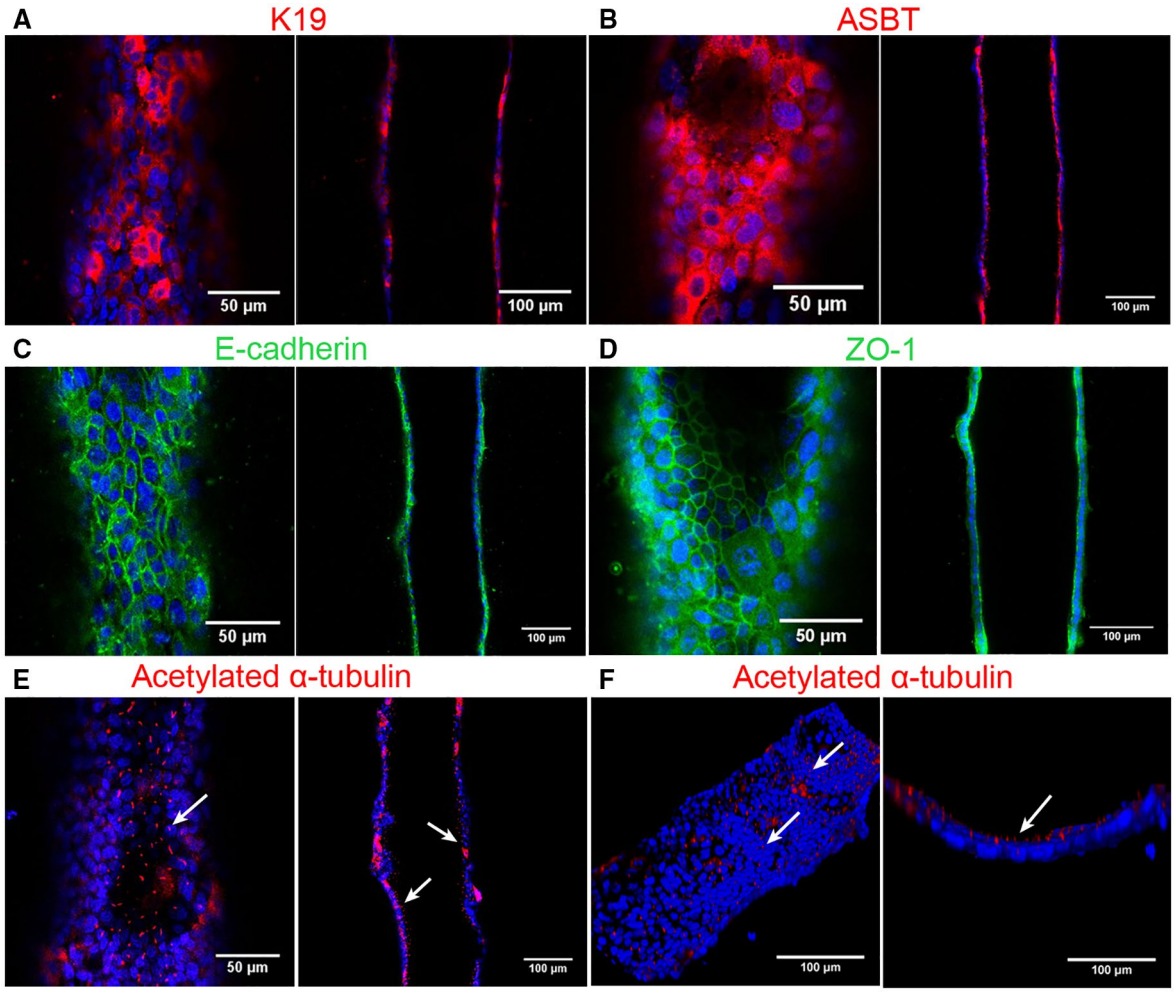

FIG. 6. Bile duct-on-a-chip with primary murine extrahepatic cholangiocytes. Immunofluorescence images across the bottom (left panels) and middle (right panels) of channels stained with antibodies (shown in red or green) against (A) K19, (B) ASBT, (C) E-cadherin, (D) ZO-1, and (E,F) acetylated α-tubulin, with DAPI nuclear staining (blue). Top (left panel, F) and cross-sectional (right panel, F) views of cilia (white arrow) in the cholangiocyte channel. Scale bars, 50 μm (left panels, except F); 100 μm (right panels and F, left panel). Images are representative of three independent experiments.

We stimulated cholangiocytes in the device with 0.1 mM of forskolin for 1 hour at 37°C with 0.2% BSA as a control. The percentage of Ki67-positive cells increased, demonstrating that forskolin promoted proliferation of both a cholangiocyte cell line and primary cholangiocytes[33] (Supporting Fig. S6), which further confirmed that cholangiocytes in the chip were functional.

Cholangiocyte functions are regulated *in vivo* by bile flow, which exerts mechanical forces on cells through primary cilia.[34-36] To test the mechanosensitivity of cholangiocytes in the bile duct-on-a-chip, we applied luminal shear flow to cells in channels using a syringe pump. First, we visualized the fluid flow field in the channel using the particle imaging velocimetry technique (Fig. 7C,D; Supporting Movie S2). By tracking the fluorescent microbeads flowing through the channel frame by frame, we were able to measure fluid velocity at different positions, which fitted well with the theoretical velocity profile calculated from steady pipe flow (Eq. 1). Then, we determined the intracellular calcium dynamics of cholangiocytes in the device. Cholangiocytes stay quiescent under static conditions and showed increased calcium signaling

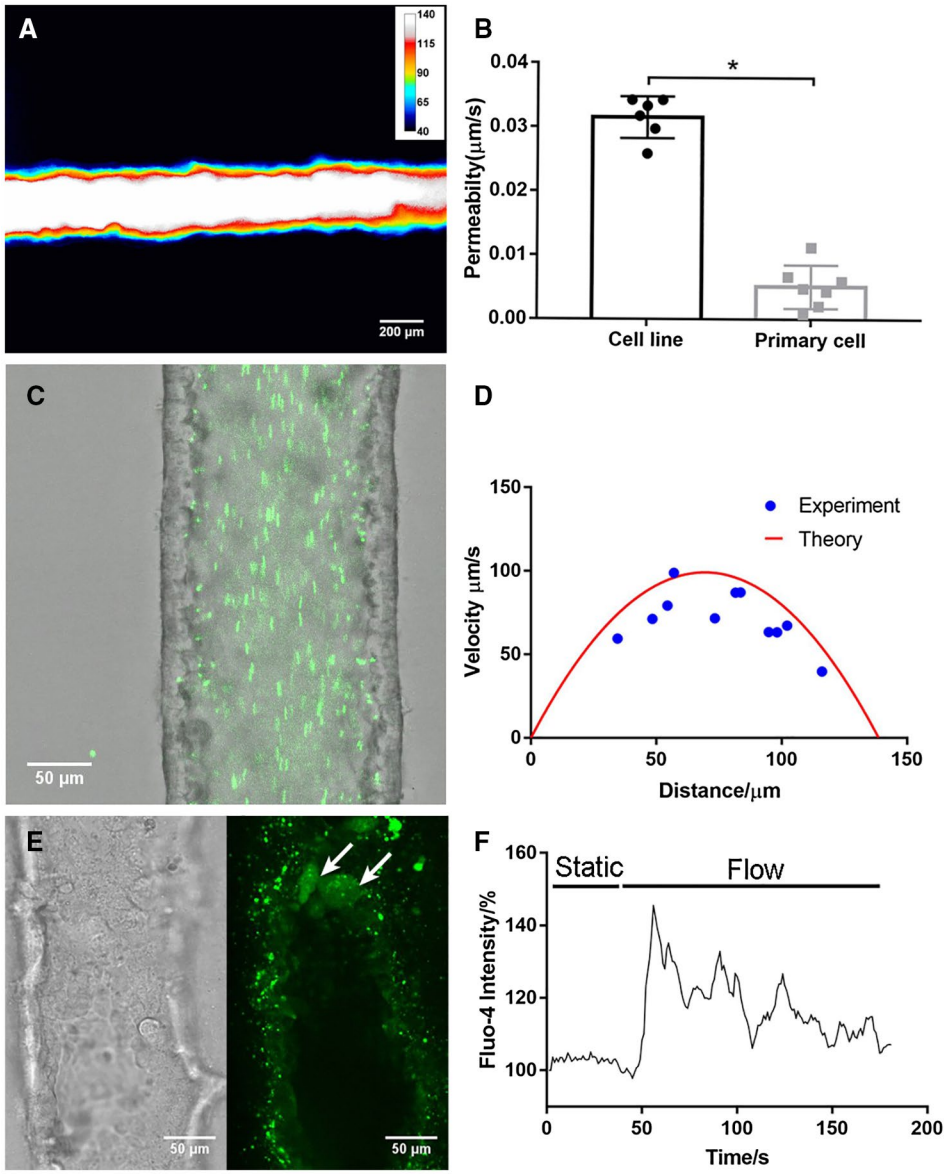

FIG. 7. A bile duct-on-a-chip constructed with primary extrahepatic cholangiocytes demonstrated better barrier function than the cell line. (A) Representative pseudo color image of FITC-dextran (4 kDa) in a channel, imaged after 10 minutes (n = 7). Scale bars, 200 μm. (B) Permeability of the cholangiocyte cell line and primary extrahepatic cholangiocyte-lined channel to 4-kDa FITC-dextran, n ≥ 6 devices. (C) Fluorescent microbeads (green, 0.2 μm) flowing through the cholangiocyte channel (cell line) at 0.02 dyne/cm^2. Scale bar, 50 μm. (D) Theoretical and experimental velocity profile of luminal fluid flow in the cholangiocyte channel at 0.02 dyne/cm^2. (E) Bright-field image and fluorescent image of activated primary cholangiocytes (white arrow) visualized with Fluo-4 fluorescence in the channel under shear flow. (F) Representative tracing of intracellular Fluo-4 fluorescence in response to luminal flow at 3.9 dyne/cm^2. All data are presented as mean ± SD; *P < 0.05.

after exposure to luminal flow (Fig. 7E); this gradually decreased after peaking (Fig. 7F; Supporting Movie S3). Thus, we demonstrated that cholangiocytes in the device are mechanosensitive, responding to luminal shear flow.

Discussion

Most *in vitro* studies of cholangiopathies have relied on 2D cell culture or on 3D organoid culture. 2D culture, although convenient, fails to replicate bile

duct physiology with respect to duct structure, ECM composition, and stiffness and does not support fluid flow. Polarized cell organization and permeability measurements, although possible, require specialized culture systems.[34,35,37] Isolated perfused intrahepatic bile duct units maintain their *in vivo* organization and have been used effectively to characterize cholangiocyte cilia as mechanical and osmotic sensors, but they do not permit measurement of monolayer permeability, manipulation of the underlying matrix, or incorporation of genetically modified or other specific populations of cholangiocytes.[36,38] Cholangiocytes in 3D spheroid culture differentiate well, can be cultured in physiological matrices, and demonstrate barrier functions and transport activities.[9-11] However, spheroids are highly variable in shape and size, and it is difficult to control their positions in a gel (for microscopy), sample lumen content, or treat the cholangiocyte apical surface. The bile duct-on-a-chip provides uniform ducts that are accessible for imaging, with two sets of ports that enable sampling of luminal contents as well as selective (apical vs. basolateral) exposures. Additionally, the chemical composition and mechanics of the surrounding matrix as well as the fluid flow rate can be varied.

Several different bioengineered bile ducts, including acellular constructs using biodegradable materials and constructs using human cholangiocytes, have been reported on. Sampaziotis et al. reconstructed the biliary epithelium with a bioengineered bile duct consisting of extrahepatic cholangiocytes derived from the common bile duct or the gallbladder.[10] These results suggested that bioengineered bile ducts may have promise for transplantation applications, but the difficulty in manipulating this duct construct makes it unsuitable for *in vitro* study. Chen et al. constructed a bile duct using organoid-derived cholangiocyte-like cells on a collagen-coated polyethersulfone hollow fiber membrane, yielding a tubular structure with polarized bile acid transport activity.[8] However, the cholangiocytes cultured on the fiber have outward-facing apical surfaces, in contrast to ducts *in vivo* and the bile duct-on-a-chip.

Previous studies have suggested that epithelial cell confluence is associated with morphology, polarity, and barrier function.[37,39-41] Although changes in transepithelial electronic resistance have been reported to be minimal after cells reach confluence,[37] we found that permeability decreased significantly when cells progressed from confluent to compact, with associated changes in height, suggesting changes in tight junction molecules.[41] These results demonstrate that compactness is required for an optimal barrier function, and suggest that confluence may be an intermediate rather than ultimate goal in the repair of an injured epithelial layer.

We demonstrated that this device can be constructed with primary murine extrahepatic cholangiocytes. Although global gene expression analysis was not performed, we showed that in the device these cells were functionally similar to cholangiocytes *in vivo*, stably expressed biliary markers, junctional molecules, and bile salt transport proteins, and developed cilia on their apical surfaces, facing the lumen. The bile duct-on-a-chip thus offers the opportunity to carry out experiments using genetically modified cholangiocytes and to compare intra- versus extrahepatic cholangiocytes. Human cholangiocytes, including those derived from induced pluripotent stem cells, could also be studied using this device.

The bile duct-on-a-chip devices are made individually and thus are difficult to use for high-throughput assays. Additionally, the limited number of cells in the device and the relatively high volume of media in the device (compared to standard tissue-culture systems) make it hard to perform traditional experiments like western blotting or to measure cholangiocyte transporter function. Although the channel diameter can be varied by varying the size of the needle used to form it, it is not possible to replicate the smallest *in vivo* ducts (several microns) because of constraints imposed by the seeding process. Despite these limitations, the bile duct-on-a-chip provides many benefits over conventional methods and has the potential to be an invaluable tool for research.

Acknowledgment: We are grateful to the UPenn Cell and Developmental Biology Microscopy Core and the UPenn NIDDK Center for Molecular Studies in Digestive and Liver Disease (NIH-P30-DK050306). This work was supported by the Center for Engineering MechanoBiology (CEMB), an NSF Science and Technology Center, under grant agreement CMMI: 15-48571 and was carried out, in part, at the Singh Center for Nanotechnology, part of the National Nanotechnology Coordinated Infrastructure Program, which is supported by the National Science Foundation grant NNCI-1542153. The small cholangiocyte cell line was generously provided by Gianfranco

Alpini (Texas A&M Health Science Center College of Medicine and Baylor Scott & White Digestive Disease Research Center).

Author Contributions: Conceptualization: Y.D., C.S.C., W.P., R.G.W. Data curation: Y.D. Formal analysis: Y.D. Funding acquisition: R.G.W. Investigation: Y.D., J.L., G.C., W.P., R.G.W. Methodology: Y.D., W.P., C.S.C., R.G.W. Resources: C.S.C., R.G.W. Supervision: R.G.W. Validation: Y.D., R.G.W. Visualization: Y.D. Writing – original draft: Y.D., R.G.W. Writing – review and editing: Y.D., J.L., G.K., W.P., C.S.C., R.G.W.

REFERENCES

1) Matsumoto K, Imasato M, Yamazaki Y, Tanaka H, Watanabe M, Eguchi H, Nagano H, et al. Claudin 2 deficiency reduces bile flow and increases susceptibility to cholesterol gallstone disease in mice. Gastroenterology 2014;147:1134-1145.e10.
2) Herr KJ, Tsang YH, Ong JW, Li Q, Yap LL, Yu W, et al. Loss of alpha-catenin elicits a cholestatic response and impairs liver regeneration. Sci Rep 2014;4:6835.
3) **Nakagawa H**, **Hikiba Y**, Hirata Y, Font-Burgada J, Sakamoto K, Hayakawa Y, et al. Loss of liver E-cadherin induces sclerosing cholangitis and promotes carcinogenesis. Proc Natl Acad Sci U S A 2014;111:1090-1095.
4) Sakisaka S, Kawaguchi T, Taniguchi E, Hanada S, Sasatomi K, Koga H, et al. Alterations in tight junctions differ between primary biliary cirrhosis and primary sclerosing cholangitis. Hepatology 2001;33:1460-1468.
5) Nakanuma Y, Tsuneyama K, Gershwin ME, Yasoshima M. Pathology and immunopathology of primary biliary cirrhosis with emphasis on bile duct lesions: recent progress. Semin Liver Dis 1995;15:313-328.
6) Zhong Y, Enomoto K, Isomura H, Sawada N, Minase T, Oyamada M, et al. Localization of the 7H6 antigen at tight junctions correlates with the paracellular barrier function of MDCK cells. Exp Cell Res 1994;214:614-620.
7) Justin AW, Saeb-Parsy K, Markaki AE, Vallier L, Sampaziotis F. Advances in the generation of bioengineered bile ducts. Biochim Biophys Acta Mol Basis Dis 2018;1864:1532-1538.
8) Chen C, Jochems PGM, Salz L, Schneeberger K, Penning LC, van de Graaf SFJ, et al. Bioengineered bile ducts recapitulate key cholangiocyte functions. Biofabrication 2018;10:034103.
9) **Vyas D**, **Baptista PM**, Brovold M, Moran E, Gaston B, Booth C, et al. Self-assembled liver organoids recapitulate hepatobiliary organogenesis in vitro. Hepatology 2018;67:750-761.
10) Sampaziotis F, Justin AW, Tysoe OC, Sawiak S, Godfrey EM, Upponi SS, et al. Reconstruction of the mouse extrahepatic biliary tree using primary human extrahepatic cholangiocyte organoids. Nat Med 2017;23:954.
11) Sampaziotis F, de Brito MC, Madrigal P, Bertero A, Saeb-Parsy K, Soares FAC, et al. Cholangiocytes derived from human induced pluripotent stem cells for disease modeling and drug validation. Nat Biotechnol 2015;33:845-852.
12) Bhatia SN, Ingber DE. Microfluidic organs-on-chips. Nat Biotechnol 2014;32:760-772.
13) Huh D, Matthews BD, Mammoto A, Montoya-Zavala M, Hsin HY, Ingber DE. Reconstituting organ-level lung functions on a chip. Science 2010;328:1662-1668.
14) Griep LM, Wolbers F, de Wagenaar B, ter Braak PM, Weksler BB, Romero IA, et al. BBB on chip: microfluidic platform to mechanically and biochemically modulate blood-brain barrier function. Biomed Microdevices 2013;15:145-150.
15) Brown JA, Codreanu SG, Shi M, Sherrod SD, Markov DA, Neely MD, et al. Metabolic consequences of inflammatory disruption of the blood-brain barrier in an organ-on-chip model of the human neurovascular unit. J Neuroinflammation 2016;13:306.
16) **Booth R**, **Kim H**. Characterization of a microfluidic in vitro model of the blood-brain barrier (muBBB). Lab Chip 2012;12:1784-1792.
17) Du Y, Li N, Yang H, Luo C, Gong Y, Tong C, et al. Mimicking liver sinusoidal structures and functions using a 3D-configured microfluidic chip. Lab Chip 2017;17:782-794.
18) Ueno Y, Alpini G, Yahagi K, Kanno N, Moritoki Y, Fukushima K, et al. Evaluation of differential gene expression by microarray analysis in small and large cholangiocytes isolated from normal mice. Liver Int 2003;23:449-459.
19) Karjoo S, Wells RG. Isolation of neonatal extrahepatic cholangiocytes. J Vis Exp 2014;88. https://doi.org/10.3791/51621.
20) Waisbourd-Zinman O, Koh H, Tsai S, Lavrut PM, Dang C, Zhao X, et al. The toxin biliatresone causes mouse extrahepatic cholangiocyte damage and fibrosis through decreased glutathione and SOX17. Hepatology 2016;64:880-893.
21) **Polacheck WJ**, **Kutys ML**, Yang J, Eyckmans J, Wu Y, Vasavada H, et al. A non-canonical Notch complex regulates adherens junctions and vascular barrier function. Nature 2017;552:258-262.
22) **Nguyen DH**, **Stapleton SC**, Yang MT, Cha SS, Choi CK, Galie PA, Chen CS. Biomimetic model to reconstitute angiogenic sprouting morphogenesis in vitro. Proc Natl Acad Sci U S A 2013;110:6712-6717.
23) Adamson RH, Lenz JF, Curry FE. Quantitative laser scanning confocal microscopy on single capillaries: permeability measurement. Microcirculation 1994;1:251-265.
24) Smith ND, Boyer JL. Permeability characteristics of bile duct in the rat. Am J Physiol 1982;242:G52-G57.
25) Tavoloni N, Wyssbrod HR, Jones MJT. Permeability characteristics of the guinea pig biliary apparatus. Hepatology 1986;6:1369-1381.
26) **Lorent K**, **Gong W**, Koo KA, Waisbourd-Zinman O, Karjoo S, Zhao X, et al. Identification of a plant isoflavonoid that causes biliary atresia. Sci Transl Med 2015;7:286ra267.
27) Boyer JL. Bile formation and secretion. Compr Physiol 2013;3:1035-1078.
28) Benedetti A, Alvaro D, Bassotti C, Gigliozzi A, Ferretti G, La Rosa T, et al. Cytotoxicity of bile salts against biliary epithelium: a study in isolated bile ductule fragments and isolated perfused rat liver. Hepatology 1997;26:9-21.
29) Xia X, Francis H, Glaser S, Alpini G, LeSage G. Bile acid interactions with cholangiocytes. World J Gastroenterol 2006;12:3553-3563.
30) Hopkins AM, Walsh SV, Verkade P, Boquet P, Nusrat A. Constitutive activation of Rho proteins by CNF-1 influences tight junction structure and epithelial barrier function. J Cell Sci 2003;116:725-742.
31) **Hohenester S**, **Wenniger LM**, Paulusma CC, van Vliet SJ, Jefferson DM, Elferink RP, Beuers U. A biliary HCO3- umbrella constitutes a protective mechanism against bile acid-induced injury in human cholangiocytes. Hepatology 2012;55:173-183.
32) Maillette de Buy Wenniger LJ, Hohenester S, Maroni L, van Vliet SJ, Oude Elferink RP, Beuers U. The cholangiocyte glycocalyx stabilizes the 'biliary HCO3 umbrella': an integrated line of defense against toxic bile acids. 2015;33:397-407.
33) Francis H, Glaser S, Ueno Y, Lesage G, Marucci L, Benedetti A, et al. cAMP stimulates the secretory and proliferative capacity of the rat intrahepatic biliary epithelium through changes in the PKA/Src/MEK/ERK1/2 pathway. J Hepatol 2004;41:528-537.

34) Li Q, Kresge C, Bugde A, Lamphere M, Park JY, Feranchak AP. Regulation of mechanosensitive biliary epithelial transport by the epithelial Na(+) channel. Hepatology 2016;63:538-549.
35) Dutta AK, Woo K, Khimji AK, Kresge C, Feranchak AP. Mechanosensitive Cl- secretion in biliary epithelium mediated through TMEM16A. Am J Physiol Gastrointest Liver Physiol 2013;304:G87-G98.
36) Masyuk AI, Masyuk TV, Splinter PL, Huang BQ, Stroope AJ, LaRusso NF. Cholangiocyte cilia detect changes in luminal fluid flow and transmit them into intracellular Ca2+ and cAMP signaling. Gastroenterology 2006;131:911-920.
37) Hidalgo IJ, Raub TJ, Borchardt RT. Characterization of the human colon carcinoma cell line (Caco-2) as a model system for intestinal epithelial permeability. Gastroenterology 1989;96:736-749.
38) Gradilone SA, Masyuk AI, Splinter PL, Banales JM, Huang BQ, Tietz PS, et al. Cholangiocyte cilia express TRPV4 and detect changes in luminal tonicity inducing bicarbonate secretion. Proc Natl Acad Sci U S A 2007;104:19138-19143.
39) Pepperkok R, Bre MH, Davoust J, Kreis TE. Microtubules are stabilized in confluent epithelial cells but not in fibroblasts. J Cell Biol 1990;111:3003-3012.
40) Ishibe S, Haydu JE, Togawa A, Marlier A, Cantley LG. Cell confluence regulates hepatocyte growth factor-stimulated cell morphogenesis in a beta-catenin-dependent manner. Mol Cell Biol 2006;26:9232-9243.
41) **Amoozadeh Y**, **Anwer S**, Dan Q, Venugopal S, Shi Y, Branchard E, et al. Cell confluence regulates claudin-2 expression: possible role for ZO-1 and Rac. Am J Physiol Cell Physiol 2018;314:C366-C378.

Author names in bold designate shared co-first authorship.

Supporting Information

Additional Supporting Information may be found at onlinelibrary.wiley.com/doi/10.1002/hep.30918/suppinfo.